Microporous and Mesoporous Materials 239 (2017) 147–157

Contents lists available at ScienceDirect

Microporous and Mesoporous Materials

journal homepage: www.elsevier.com/locate/micromeso

Co/MCM41 catalyst in the COProx reaction prepared by supercritical CO_2 reactive deposition

Soledad G. Aspromonte [a, *], Martín D. Mizrahi [b], Esther Alonso [c], José M. Ramallo-López [b], Alicia V. Boix [a]

[a] Instituto de Investigaciones en Catálisis y Petroquímica – INCAPE (FIQ, UNL-CONICET), Santiago del Estero 2829, 3000, Santa Fe, Argentina
[b] Instituto de Investigaciones Fisicoquímicas Teóricas y Aplicadas – INIFTA (CCT La Plata – CONICET, UNLP), Diagonal 113 y calle 64, 1900, La Plata, Argentina
[c] High Pressure Processes Group – Chemical Engineering and Environmental Technology Department, University of Valladolid, C/ Dr. Mergelina s/n, 47011, Valladolid, Spain

ARTICLE INFO

Article history:
Received 8 August 2016
Received in revised form
7 October 2016
Accepted 8 October 2016
Available online 11 October 2016

Keywords:
COProx
Mesoporous
Supercritical deposition
Template-ion exchange
EXAFS/XANES

ABSTRACT

Co/MCM41 catalyst with 4.3 wt % Co (Co/sc) has been prepared by supercritical CO_2 reactive deposition ('scfrd') and characterized by different physicochemical techniques. This synthesized method was compared with others conventional methodologies such as template-ion exchanged (Co/tie) and incipient wet impregnation (Co/iwi) with similar cobalt content. All the samples were studied as catalysts on the CO total oxidation (COTox) and preferential oxidation of CO on H_2-rich streams (COProx). Incorporating cobalt with supercritical CO_2 leads to a catalyst which produces values of CO conversion similar to those obtained by conventional methods such as incipient wetness impregnation (Co/iwi) or template-ion exchanged (Co/tie). It has been possible to identify different cobalt species present in catalysts depending on their synthesis methods by Temperature-Programmed Reduction (TPR), X-ray Photoelectronic (XPS), Laser Raman (LRS) and X-ray Absorption (XANES/EXAFS) spectroscopic studies. All samples containing a main cobalt species of cobalt (II) coordinated with Si tetrahedral sites form part of mesoporous structure and lesser extent, cobalt orthosilicate on the surface. In addition, Co_3O_4 species dispersed over the MCM41 support were detected for the Co/iwi and Co/sc catalysts.

Thus, the combination of Co_3O_4 nanoparticles and Co(II) sites interacting with the siliceous structure, highly dispersed on the surface and inside the mesoporous support obtained by the 'scfrd' method resulted in a more active and selective catalyst for the COProx reaction.

1. Introduction

TheMCM-41 material is one of the most representative members of the mesoporous structures, characterized by a one-dimensional structure of uniform cylindrical mesopores of about 2–10 nm organized in a hexagonal symmetry [1,2]. The highly ordered pore systems with tunable pore sizes [3], large surface areas and pore volumes, as well as a high density of surface silanols [4] provide excellent opportunities in chemistry, catalyst and separation processes [5,6].

Many efforts have been devoted to expand the application of mesoporous silica materials as catalysts with tunable properties. In this sense, the introduction of various metal cations provides great potential. Likewise, it has been found that, depending on the preparation method used, the metal ion can be incorporated in the framework of the mesoporous silica matrix or can occupy extra-frame positions [7,8]. Initially, the incorporation of aluminum into the MCM41 structure was performed to create acidity in the material [9,10]. In addition, the MCM41 material with V, Fe, Mn, Cs and others metals has been successfully synthesized [11–14]. Similarly, the incorporation of heteroatoms such as Cu, Zn, Al, B, Ga, Fe, Cr, Ti, V, Co and Sn into the mesoporous silica framework has been extensively investigated [15,16]. The incorporation of transition metals as cobalt or copper into mesoporous materials is of considerable interest because Co and Cu catalysts are widely used in many processes, particularly those of environmental importance, and they constitute a cheap alternative to the use of noble metals as active centers of catalysts for the oxidation and reduction reactions.

* Corresponding author.
E-mail address: saspromonte@fiq.unl.edu.ar (S.G. Aspromonte).

http://dx.doi.org/10.1016/j.micromeso.2016.10.006
1387-1811/

In this sense, the preferential oxidation of CO (COProx) has recently raised considerable interest as an alternative route for the removal of CO from hydrogen-rich streams used to PEM fuel cells (Proton Exchange Membrane Fuel Cells) [17]. Before entering the cell, the CO concentration must be less than 10 ppm in order not to deteriorate the cell anode. Therefore, numerous articles on transition metal oxides such as Cu–Ce and Co–Ce systems have been published, in which oxides play a fundamental role in redox reactions [18,19].

On the other hand, some catalysts have been reported which are based on noble metals highly dispersed in mesoporous supports. Wang et al. [20] reported Ru catalysts supported on different mesoporous silica, MCM-41, MCM-48, SBA-15 and KIT-6. The performance of Ru catalysts in the COProx reaction was related to the Ru dispersion and reducibility, and support pore structure. Following this line of research, Huang et al. [21] reported high activity and selectivity of Pt supported on mesoporous substrate (FSM-16) for the PROX reaction.

The behavior of systems $CuO–CeO_2$ on SBA-15 active and selective in the oxidation of CO has recently been published [22]. This catalyst showed high CO conversion with 5 wt % of copper.

The deposition of catalytically active nanoparticles on supports with high dispersion is an important and effective strategy for the design of catalysts. Conventional methods such as impregnation techniques often generate agglomerations or large particles with broad size distribution in the mesopores and/or on the external surface of the porous catalyst. The incipient wetness impregnation ('iwi') method allows a good control on metal loading but a poor control on metallic dispersion [23,24]. Thus, it is important to study and analyze different ways to introduce the active phase in the mesoporous support. The MCM41 materials are synthesized in alkaline media by the so-called (S^+I^-) synthesis route [25], where S^+ is the cationic surfactant and I^- is the anionic inorganic silica precursor [26,27]. The template ion exchange ('tie') method is based on the concept that the cationic surfactants in the as-synthesized mesoporous materials can be partially replaced through ion exchange by other inorganic cations. Metal ions ($M^{\delta+}$) such as Ag^+, Mn^{2+}, VO^{2+}, Fe^{3+} and Cr^{3+} have been introduced into MCM41 by the 'tie' method [28–32]. These catalysts were employed for oxidation reactions such as the oxidation of CO [28], methane [31] and short-chain alkanes (ethylene and propylene) [32]. Since there are no cation-exchange sites in the purely siliceous MCM41 after calcination, it is difficult for the metal components to be exchanged as in the exchanged zeolites sites [33,34].

Furthermore, an interesting method for incorporating active phases on catalyst supports is the reactive deposition using supercritical fluids ('scfrd'). It is a promising method to deposit nanoparticles and films on inorganic porous supports, polymer substrates and carbon nanotubes [35,36]. This process involves the dissolution of an organometallic precursor in a supercritical fluid (SCF), the impregnation of the substrate by exposure to this solution, and the subsequent decomposition of the precursor. CO_2 is the most commonly used supercritical fluid ($scCO_2$) for material synthesis because it is non-toxic, non-reactive, nonflammable and inexpensive. Under supercritical conditions, CO_2 as a solvent has intermediate properties between gases and liquids. The gas-like diffusivity and viscosity of $scCO_2$ are favorable for rapid diffusion and permeation into mesoporous substrates, whereas the liquid-like density allows the dissolution of a wide range of organometallic precursors. The zerosurface tension of $scCO_2$ allows a better penetration and wetting of pores than liquid solvents and avoids the pore collapse which can occur on certain structures. The simple removal from the substrateby controlled decompression is performed without leaving any residue on the support [37–39].

The goal of the present study is to investigate the cobalt species which are incorporated in the MCM41 catalytic support by different synthesis methods and compare its catalytic properties in the CO Preferential Oxidation reaction. The methods used to incorporate the active phase was (i) template-ionic exchange ('tie'), (ii) incipient wet impregnation ('iwi') and (iii) supercritical CO_2 reactive deposition ('scfrd') in the total and preferential CO oxidation in reductive atmosphere to purify H_2 streams. Spectroscopic methods such as X-ray absorption (EXAFS/XANES), X-ray photoelectron (XPS) and Laser Raman (LRS) together with temperature-programmed reduction (TPR) techniques are used to characterize the nature and local environment of the cobalt sites in these types of materials.

2. Experimental section

2.1. Synthesis of MCM41

The MCM41 support was synthesized following the method used by Szegedi et al. [40]. A solution of surfactant (C_{16}TMABr) was prepared by continuous mixing with de-ionized water and absolute ethanol at room temperature. The pH of the solution was adjusted by adding an aqueous ammonia solution (29 wt %). Then, tetraethylorthosilicate (TEOS) was added dropwise in a couple of minutes. The molar composition of the resulting gel mixture was $TEOS:0.3C_{16}TMABr:11NH_3:144H_2O:58EtOH$.

The support thus obtained was filtered, thoroughly washed with de-ionized water and dried for 12 h at 60 °C. The template was removed by calcination in a flow of air at 550 °C during 6 h.

2.2. Incorporation of cobalt

Template-ion Exchange ('tie' method). For the TIE synthesis, 1 g of the as-synthesized MCM-*as* containing the template was added to a solution of cobalt nitrate 0.1 M. The exchange was carried out at room temperature for 24 h under intense stirring. The exchanged suspension was filtered, thoroughly washed with deionized water, and then dried at 80 °C. The removal of the organic template ions was achieved by calcination in air flow, heating from room temperature to 550 °C at a rate of 2 °C·min^{-1} and kept at 550 °C for 6 h in air flow. The cobalt content was 2.6 wt %, which was determined by Inductively Coupled Plasma (ICP-OES). The catalyst prepared by the 'tie' method will be referred to as 'Co/tie'.

Incipient wetness impregnation ('iwi' method). The impregnated Co/iwi sample was prepared by mixing the calcined MCM41 support with an aqueous solution of cobalt acetate [$(Co)(C_2H_3O_2)_2(4H_2O)$] 2 M to get 3 wt % of cobalt. The volume of solution used was the one which was necessary to completely wet the mesoporous sample. The solution temperature was room temperature. Then, the sample was dried at 110 °C and calcined at 550 °C in air flow for 6 h. The Co-promoted MCM41 prepared by impregnation will be referred to as 'Co/iwi'.

Supercritical CO_2reactive deposition ('scfrd'). We have already reported the deposition of cobalt [41,42]. Cobalt (II) bis-(η^5-cyclopentadienyl), also known as cobaltocene ($CoCp_2$) was used as cobalt precursor. The deposition reaction was carried out in a high-pressure stainless steel reactor with an effective volume of 100 ml. A certain amount of MCM41 support (100 mg) was located in a glass tube of 15 mm in diameter inside the reactor vessel, together with another smaller tube (6 mm in diameter) with the cobalt precursor. Both tubes were separated by a wire mesh to allow the entry and circulation of $scCO_2$. The reactor was equipped with two wall resistances positioned at the bottom of the reactor to promote the convective flow of $scCO_2$. The initial amount of cobaltocene was 0.48 g L^{-1} in all the experiments.

The deposition experiments were carried out in batch operation divided into two consecutive stages. During the first step, the dissolution of the $CoCp_2$ precursor in $scCO_2$and the impregnation of the support occurred, and operational conditions were fixed at 70 °C and 110 bar during 3 h. The second step was the decomposition and deposition at 200 °C and 160 bar. After 3 h, the $scCO_2$ was released from the reactor over a period of approximately 1 h, which implied a slowly depressurization up to atmospheric pressure. The Co-MCM41 prepared with supercritical CO_2 will be referred to as 'Co/sc'.The cobalt loading in the final material was determined by Inductively Coupled Plasma (ICP-OES) and it was of 4.3 wt % Co.

2.3. Physicochemical characterization

2.3.1. Textural and chemical properties

Nitrogen physisorption isotherms were measured at −196 °C using a Quantachrome Autosorb instrument. Prior to adsorption, the samples were degassed at 350 °C for 6 h (10^{-4} Torr). Specific surface areas were calculated from the linear region of BET plots [43], while the total pores volume was calculated using the BJH method [44].

In addition, the small angle X-ray scattering (SAXS) analyses were performed in a Hecus-Braun chamber. This equipment was installed on a PANanlytical X-ray generation model PW3830. Measurements were carried out at 2θ between 0° and 8°. The interplanar distance in the (1 0 0) direction, 'd_{100}' was calculated by Bragg's Law ($\lambda = 2d_{hkl} \sin\theta$) and the unit cell parameter 'a_0' was also obtained, indicating the distance between the center of two adjacent pores in the hexagonal structure ($a_0 = 2\ d_{100}/\sqrt{3}$) [45].

2.3.2. Morphology characterization

The catalysts were characterized in a JEOL JEMARM200F electron microscope. STEM images were simultaneously recorded in both the HAAF and BF modes with the microscope operated at 200 kV. The samples were dissolved in methanol and were placed in a carbon grid to be directly introduced into the microscope. This technique was used to determine the organization, morphology and dimension of nanoparticles, as well as to observe the presence of these particles dispersed inside and/or outside the pores.

In addition, the application of scanning electron microscopy (SEM) combined with detection energy dispersive X-ray spectroscopy (EDX) was performed to determine the chemical composition of the deposited particles. An environmental scanning electron microscope (ESEM) FEI Quanta model 200FEG operating at 30 kV was used. Besides, a backscattered electron detector was used to observe the Co nanoparticles. This detector in particular was able to measure in Z contrast, i.e. the contrast related to the atomic number (Z) of the element upon which the beam impinges. Therefore, if there were phases with different Z of higher values, they would be brighter than the other phases.

2.3.3. Reducibility of Co species

Temperature-Programmed Reduction (TPR) measurements were carried out using an Okhura TP-2002S instrument equipped with a TCD detector. Samples were heated at 10 °C·min^{-1}in inert flow up to the calcination temperature and kept constant at this temperature for 2 h. Next, they were cooled to room temperature and stabilized in H_2 (5%)/Ar. The temperature and detector signals were then continuously recorded while heating at 10 °C·min^{-1} up to 900 °C.

2.3.4. Spectroscopies

Raman spectra were recorded in a Horiba JOBIN YVON Lab RAM HR instrument. The excitation source was the 514.5 nm line of a Spectra 9000 Photometrics Ar ion laser with the laser power set at 30 mV. The powder sample was pressed at 4 bar into self-supporting wafers.

X-ray absorption spectroscopy (XAS) experiments at the Co K edge (7709 eV) were performed at the XAFS2 beamline at the LNLS (Laboratorio Nacional de Luz Sincrotron) in Campinas, Brazil. The XAS spectra were collected in the XANES (X-ray absorption near edge structure) and EXAFS (Extended X-ray absorption fine structure) regions at room temperature using a Si (111) single channel-cut crystal monochromator in transmission mode, and with three ion chambers as detectors. The samples were placed between the first and the second ion chambers and the third one was used to measure the corresponding metallic reference simultaneously with the samples. Moreover, the XAS spectra of reference compounds, Co(0), Co_3O_4 and CoO, were also collected. The Co(0) metallic used is a metal thin film manufactured by the company EXAFS Materials. For oxide references, the respective powder (Sigma Aldrich) is used.The appropriate quantities of material were calculated in order to obtain an edge jump $\Delta\mu x$ near 1, with a total absorbance after edge $\mu x(E) < 2$. The samples were pressed under 0.5 MPa into pellets of 12 mm of diameter.

The EXAFS data was extracted from the measured absorption spectra by standard methods using the ATHENA software which is part of the IFEFFIT package [46]. The Fourier transforms were calculated using the Hanning filtering function. The EXAFS modeling was carried out using the ARTEMIS program (IFEFFIT package). Structural parameters (coordination numbers and bond lengths and their mean squared disorders) were obtained by a nonlinear least-squares fit of the theoretical EXAFS signal to the data in R space by Fourier Transforming both the theory and the data. Theoretical scattering path amplitudes and phase shifts for all paths used in the fits were calculated using the FEFF code [47]. The *k*-range was set from 2 to 14 $Å^{-1}$ and the Fourier transforms were fitted in the region 1–3.5 Å. The passive reduction factor S_0^2 was restrained to the value of 0.78. This value was obtained fitting the EXAFS spectrum of metallic Co foil constraining the coordination number of the first coordination shell to 12.

In addition, the surface features of the catalysts were studied in a multitechnique system (SPECS) equipped with a dual Mg/Al X-ray source and a hemispherical PHOIBOS 150 analyzer operating in the fixed analyzer transmission (FAT) mode. The spectra were obtained with a pass energy of 30 eV and the Al Kα X-ray source was operated at 200 W and 12 V. The working pressure in the analyses was less than 5.9×10^{-7} Pa. The spectral regions corresponding to Si 2p, O 1s, Co 2p and Si 2s core levels were recorded for each sample. The static charge of the samples was corrected by referencing all binding energies (BE) to the C 1s peak (BE ~ 284.6 eV). In addition, the Si 2p peak at 103.0 ± 0.1 eV binding energy was taken as an internal reference. The data treatment was performed with the CASA XPS program (Casa Software Ltda., UK). The areas of the peaks were computed by fitting the experimental spectra to Gaussian/Lorentzian curves after removing the background (using the Shirley function). In particular, the deconvolution of the main peaks for Co 2p region was made considering that the ratio between the $2p_{3/2}$ and $2p_{1/2}$ areas was equal to 2. The same criterion was maintained for satellite peaks. Surface atom ratios were calculated from peak area ratios normalized by means of the corresponding atomic sensitivity factors.

2.4. Catalytic performance

The calcined catalysts were tested in the COProx (Preferential CO oxidation) and COTox(Total CO oxidation) reactions. These processes were selected such as test reactions in order to analyze the influence of different methods of synthesis on the catalytic activity.The tests were performed in a fixed-bed flow reactor at

atmospheric pressure. The reaction mixture was composed of 1% CO, 1% O_2 and/or 40% H_2in He balance. The catalyst weight/total flow ratio was 2.1 mg cm^3 min^{-1}. The CO conversion and selectivity towards CO_2 were defined as:

$$x_{CO}\ (\%) = \frac{100\ (CO^{\circ} - CO)}{CO^{\circ}} \quad (1)$$

$$S\ (\%) = \frac{50\ (CO^{\circ} - CO)}{O_2{}^{\circ} - O_2} \quad (2)$$

where CO, O_2 are the reactor exit concentrations and CO°, $O_2{}^{\circ}$ represent the feed concentrations, which were measured with a GC-2014 Shimadzu chromatograph equipped with a TCD detector. All the catalysts were first evaluated in the COProx and then, in the COTox reaction.

3. Results and discussion

3.1. Physical and chemical properties of mesoporous materials

Nitrogen physisorption is a routine technique to probe the texture of porous solids. All the synthesized catalysts presented a type IV isotherm (see Fig. S1, supplementary Material) according to the IUPAC nomenclature [48], which is typical for MCM41 mesoporous materials [49,50].

For all samples, a sharp step in the range of relative pressures between 0.18 and 0.30 is observed, which indicates the filling of rather uniform mesopores by capillary condensation. The position of the pore-filling riser points towards pore diameters in the lower range of what is typically found for MCM41 materials.

Table 1 presents the quantitative results obtained from the N_2 adsorption-desorption isotherms for the MCM41 support and cobalt catalysts. In addition, the interplanar distance and unit cell parameter obtained from the SAXS diffractograms are also shown.

The mesoporous support presents a surface area and pore volume of 1295 m^2g^{-1} and 0.50 cm^3g^{-1}, respectively.The addition of 4.3 wt % of cobalt by $scCO_2$ produced a decrease of 20% of surface area due to the cobalt incorporation on the silica structure. However, when the method employed to incorporate cobalt was template-ionic exchange or incipient wet impregnation, the surface area decreased to 545 or 380 m^2g^{-1}, respectively. In both cases, the amount of cobalt incorporated into the structure was less than that obtained by supercritical method; however the damage of siliceous structure with loss of surface and pore volume was significant, due to low hydrothermal stability in the presence of aqueous medium.

Accordingly, to determine the channel arrangements of the mesoporous materials, the small angle X-ray scattering (SAXS) technique was employed. The regular arrangement pores produce reflections that appear as signals at low diffraction angles. Fig. 1 shows the SAXS diffractograms obtained for all the calcined catalysts. The purely siliceous parent material (Fig. 1a) gives a well-defined diffraction pattern with an intense diffraction peak at $2\theta = 2.2^{\circ}$, characteristic of the (100) reflection plane which indicates an ordered pore structure of MCM41 support. In addition, the weak diffraction peaks close to 4.3 and 5.0°, which are attributed to the (110) and (200) planes confirm the synthesized mesoporous structure. These are typical characteristics indicating that a good-quality MCM41 material with hexagonal long-range order has been obtained [51].

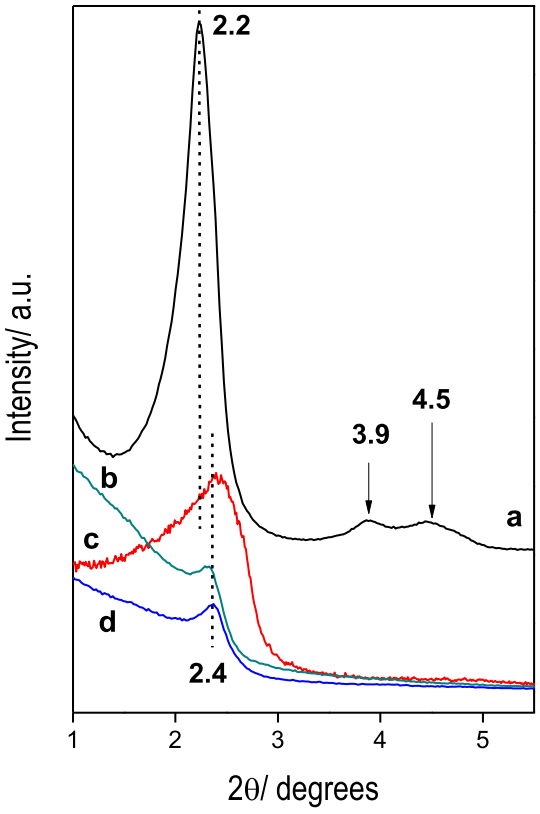

Fig. 1. Small angle X-ray scattering pattern of (a) MCM41, (b) Co/tie, (c) Co/sc and (d) Co/iwi samples after calcination.

Instead, the incorporation of cobalt produced a gradual shift of the main peak to higher values of 2θ~2.4°, which would indicate a loss of the original periodicity. The decrease of the (100) reflection intensity and the lack of (110) and (200) peaks are related to a loss of hexagonal arrangement structure. From SAXS data it is possible to estimate the characteristic parameters such as the interplanar distance 'd_{100}' and the unit cell parameter 'a_0'. Note that both parameters decrease slightly, which indicates that the distance between the centers of two adjacent pores remains practically constant after the incorporation of cobalt.

In accordance with the textural results as well as those obtained by SAXS, incorporating cobalt with the use of aqueous synthesis medium, conducted to the loss mesoporous order and the significant decrease of the surface area and pore volume, which can be linked to the hydrolysis of Si—O—Si bonds, intense capillary stress exerted in water and the cobalt loading. Probably, there is a combination of effects involving chemical and mechanical resistance, as well as the cobalt content incorporated, producing the deformation of the structure, more accentuated to the 'tie' and 'iwi' methods [52,53]. However, the methodology employing supercritical CO_2 conducted in dry conditions avoid this effect.

Table 1
The structural and textural properties of calcined catalysts.

Catalysts	% Co[a]	S_{BET}[b]	V_p[c]	d_{100}[d]	a_0[e]	Pore size[f]
MCM41	0	1295	0.50	4.0	4.6	4.6
Co/tie	2.6	545	0.45	3.8	4.4	4.0
Co/iwi	3.0	380	0.22	3.8	4.4	4.2
Co/sc	4.3	1034	0.35	3.7	4.3	3.9

[a] Cobalt content (wt. %) measured by ICP-OES.
[b] Surface area, calculated from N_2 isotherms/m^2g^{-1}.
[c] Porous volume calculated from BJH method/cm^3g^{-1}.
[d] Interplanar distance, $d_{100} = \lambda/2 \sin\theta$/nm.
[e] Unit cell parameter, $a_0 = 1.1547\ d_{100}$/nm.
[f] Average pore size/nm.

3.2. Morphological analysis

The morphology of catalysts was illustrated by SEM and HAAF-STEM analyses, as shown in Fig. 2. The micrograph of MCM41 (Fig. 2A) shows a uniform spherical morphology with a homogeneous size distribution centered on 500 nm. The spherical morphology of the MCM41 particles and the sphere size are retained after the cobalt incorporation through any of the methods used in this work.

Therefore, it is important to note that by the incipient wet impregnation and the supercritical CO_2 methods (Fig. 2C and D), nanoparticles were observed with a diameter close to 20 nm homogeneously distributed over the mesoporous spheres. In the HAAF-STEM image bright patches are observed (Fig. 2C), which indicate high electron dense areas, where increased brightness is due to the presence of cobalt. The areas of high electron density appear well dispersed and correspond to cobalt nanoparticle with approximately 20 nm of diameter. The EDX results indicated the presence of cobalt inside and outside of the spheres.

An important difference was observed in the Co/tie catalyst (Fig. 2B). A thin film on the surface of the spheres was developed after exchanging the cobalt with template ions. This feature was detected over all the spheres formed and it was observed by other authors, i.e. γ-Fe_2O_3 nanoparticles were incorporated by the sol-gel method on the MCM-41 support [54] or after the functionalization with polyethylenimine (PEI) [55].

For the purpose of determining the nature of the film in the surface of the spheres, the EDX profile along the radial line was measured (Fig. 3A). The signals correspond to CoK, CoL and SiK edges from the outer surface to center were recorded (Fig. 3B).

The signals corresponding to cobalt K and L edges increase with the distance to center, reaching a maximum value at 0.025 μm, and then decrease and remain constant for longer distances. The signal due to Si–K continuously increases towards the interior of the mesoporous sphere. These results suggest that the cobalt was homogeneously distributed in the interior of the sphere, but also located preferentially in the outer surface.

Probably, this effect is produced by the nature of the synthesis process. The ionic-exchanged method involves the exchange between the Co(II) ions by the cationic surfactant which is present in the sample before the calcination. When begins the exchanged ion, the pores are filled with bulky surfactant molecules. Therefore, there is a limitation or restriction for the diffusion of cobalt precursor into the spheres.

3.3. Characterization of cobalt species

Fig. 4 presents the temperature-programmed reduction (TPR) profiles of the Co-MCM41 samples. The Co/tie catalyst (Fig. 4a) presents a single reduction peak at 787 °C, which corresponds to Co ions in high interaction with the silica structure. In this sense, Lim et al. [56] reported the formation of cobalt silicate during the calcination at different temperatures of the Co-MCM41 samples with 1 and 4 wt % Co. They observed a single peak of reduction above 700 °C assigned to cobalt orthosilicate (Co_2SiO_4) as the main species on the Co-MCM41 sample after calcination at 900 °C for 1 h.

On the other hand, the Co/iwi and Co/sc catalysts (Fig. 4b and c, respectively) show two reduction regions at lower temperature from 200 to 400 °C which correspond to cobalt oxide species. The TPR profile of the Co/SiO_2 reference sample reported by Boix et al.

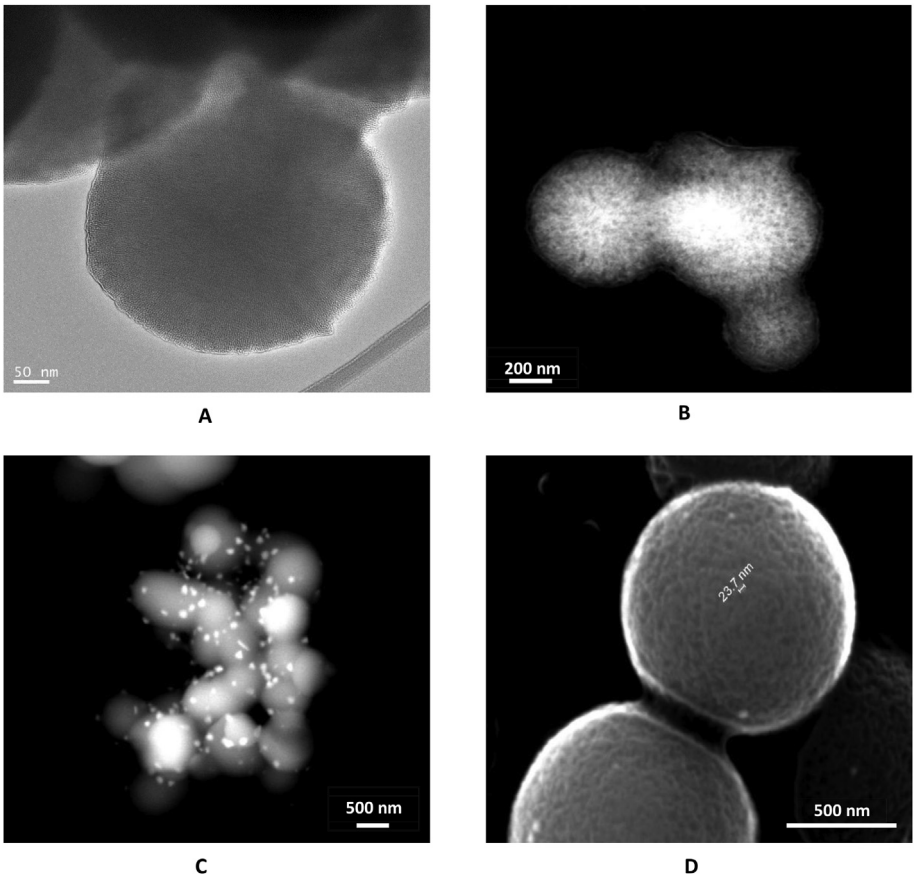

Fig. 2. SEM images of (A) MCM41, (D) Co/sc and HAAF-STEM images of (B) Co/tie, (C) Co/iwi catalysts.

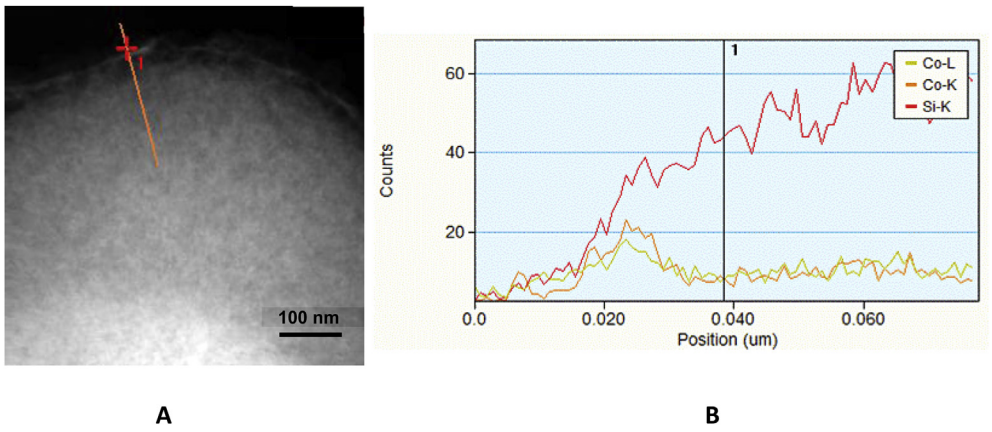

Fig. 3. (A) SEM images of Co/tie sample and (B) EDX results along the orange line. (For interpretation of the references to colour in this figure legend, the reader is referred to the web version of this article.)

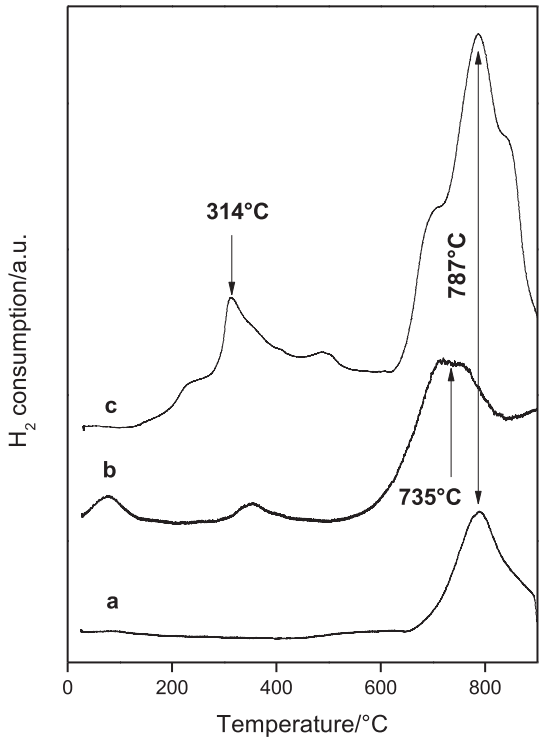

Fig. 4. TPR profiles obtained for (a) Co/tie, (b) Co/iwi and (c) Co/sc catalysts.

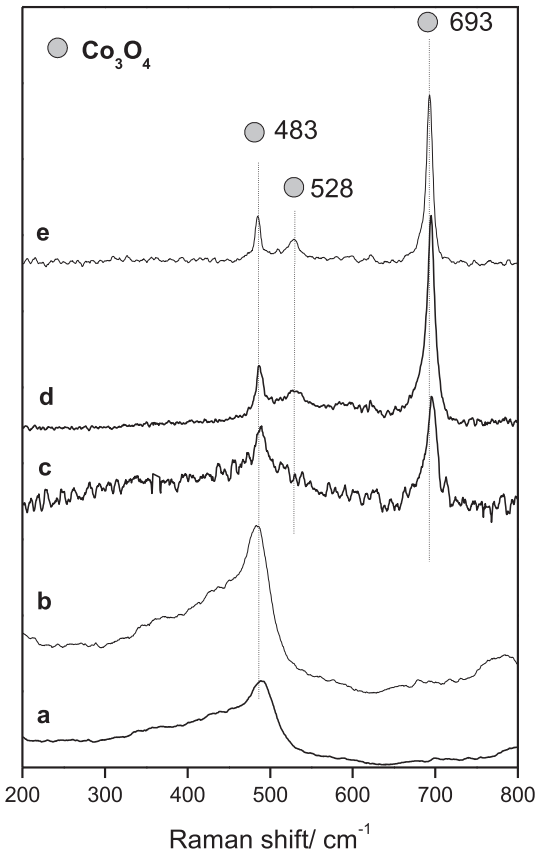

Fig. 5. Raman spectra of (a) MCM41, (b) Co/tie, (c) Co/iwi, (d) Co/sc and (e) Co/SiO_2 samples.

[57] showed the complete reduction of the Co_3O_4 phase at less than 400 °C in agreement with other literature data [58–61]. In Fig. 4c, shoulders next to the main peak at 314 °C suggest the presence of Co_3O_4 particles with different size dispersed in the silica structure. In addition, a very intense peak at higher temperature (~787 °C) is related to Co(II) species linked to silanol groups in the silica structure [56]. The hydrogen consumption ratio in the (low:high) temperature region resulted equal to 30:70 for the Co/sc catalyst.

The formation of Co_3O_4nanoparticles was favored by oxidizing nature of atmosphere of synthesis, where the cobalt deposition by supercritical CO_2 at elevated temperature and pressure promotes the oxidation of organic cobalt precursor.

Fig. 5 presents the Raman spectra of the MCM41 (Fig. 5a), Co/tie (Fig. 5b), Co/iwi (Fig. 5c), Co/sc (Fig. 5d) and a reference sample (Fig. 5e) with 3.2 wt % Co_3O_4 on SiO_2 (20 m^2g^{-1}) prepared by impregnation (denoted as Co/SiO_2). The MCM41 support and Co/tie catalyst show a broad band centered at about 483 cm^{-1} correspond to the oxygen vibration of the Si–O–Si linkage as reported in the literature for amorphous silicas [62,63]. The main Raman peaks observed for Co/SiO_2 corresponds to the E_g (483 cm^{-1}), F_{2g} (528 and 621 cm^{-1}), A_{1g} (693 cm^{-1}) modes of the Co_3O_4 crystalline phase and are consistent with previous investigations [64–66]. In agreement with TPR results, the spectra of the Co/iwi and Co/sc samples present the main peak at 693 cm^{-1} and a slight one at 528 cm^{-1}, both of them corresponding to a less developed Co_3O_4

phase. Probably, the signal at 483 cm^{-1} is overlapped with the MCM41 support. It is important to remark that the bands assigned to CoO species (455 and 675 cm^{-1}) are not observed [66].

The EXAFS technique is a powerful method for studying the structure of materials, because it provides information about the local environment of selected elements in the samples studied [67].Through this technique, the distance to the backscattering neighbors may be determined, as well as their identity. Fig. 6 shows the EXAFS oscillations at the Co K-edge of the catalysts prepared by the three different methods.

Two of them show very similar oscillations: the catalyst prepared by incipient wet impregnation (Fig. 6a) and by the 'tie' method (Fig. 6b). In contrast, the catalyst prepared by $scCO_2$ shows a different EXAFS signal (Fig. 6c).

The amplitudes of the Fourier transforms can be seen as a pseudo-radial distribution function of atoms and give preliminary and qualitative information of the surroundings of the absorber atom. The two catalysts that showed similar EXAFS oscillations have two peaks in the Fourier transforms at 1.5 and 3.0 Å, approximately (without phase correction). These can be seen as two coordination spheres around Co atoms (Fig. 6d and e). In this sense, the catalyst Co/sc (Fig. 6f) shows a contribution at 1.5 Å as the other catalysts, but the region above 2 Å presents a more complex structure with various unresolved peaks what could be indicating a mixture of Co species.

In order to obtain quantitative information about the surrounding shells of Co atoms, the EXAFS oscillation fits were performed using the IFEFFIT package [68]. Phases and amplitude functions were generated by the FEFF code [69]. From the EXAFS analysis data, the type of neighboring atoms and the distance between them could be determined. EXAFS is a well-suited method for providing a direct proof of the incorporation of metals such as cobalt into the framework of mesoporous materials. The most crucial factor is the identification of the neighbors to Co atoms, which should be oxygen in the first shell and Si in the second shell.The quantitative results of the fits are shown in Table 2 and Fig. 6d and e (solid lines). It is important to note that it was not possible to obtain a satisfactory fit of the spectrum corresponding to the Co/sc catalyst, probably due to the presence of different cobalt environments. For this reason, the structural analysis will be performed later from the XANES region of the Co K-edge absorption spectrum. The results of the EXAFS fits show that the catalysts prepared by the 'iwi' and 'tie' methods have a very similar atomic structure around Co. In both catalysts, the first peak of the Fourier Transform corresponds to two shells of oxygen atoms, one of approximately 4 atoms at 2.10 Å and another one of 0.4 oxygen atoms at a shorter distance. This last shell could be assigned to the presence of water molecules around some Co atoms [70].The other coordination sphere corresponds to Si atoms at a distance of 3.4 Å, approximately. In this sense, no cobalt shells were found in the fits for any of these catalysts, which suggest that no cobalt oxide or metallic cobalt is present. These results indicate that in these catalysts Co atoms are incorporated into the MCM41 framework, occupying Si tetrahedral sites [71].Therefore, linking these results with those obtained from the TPR profiles, there is a fraction of cobalt (II) located within the mesoporous structure and coordinated with Si tetrahedral sites.

Fig. 7 shows the XANES spectra obtained at the Co K-edge of all catalysts and some reference materials. In agreement with EXAFS results (Fig. 6), Co/iwi and Co/tie catalysts have similar XANES profiles. In contrast, the one prepared by supercritical fluid presents a different XANES spectrum.

Table 2
Results obtained from the EXAFS fits.

Catalysts	Pair	N[a]	R[b]/Å	σ^{2c}/Å^2
Co/iwi	Co–O	0.4 ± 0.1	1.99 ± 0.03	0.002 ± 0.001
	Co–O	4.0 ± 0.8	2.11 ± 0.03	0.009 ± 0.001
	Co–Si	4.1 ± 0.6	3.40 ± 0.04	0.003 ± 0.001
Co/tie	Co–O	4.5 ± 0.6	2.07 ± 0.02	0.007 ± 0.002
	Co–Si	4.6 ± 0.8	3.37 ± 0.04	0.003 ± 0.001

[a] Average coordination number.
[b] Interatomic distance.
[c] Debye-Waller factor.

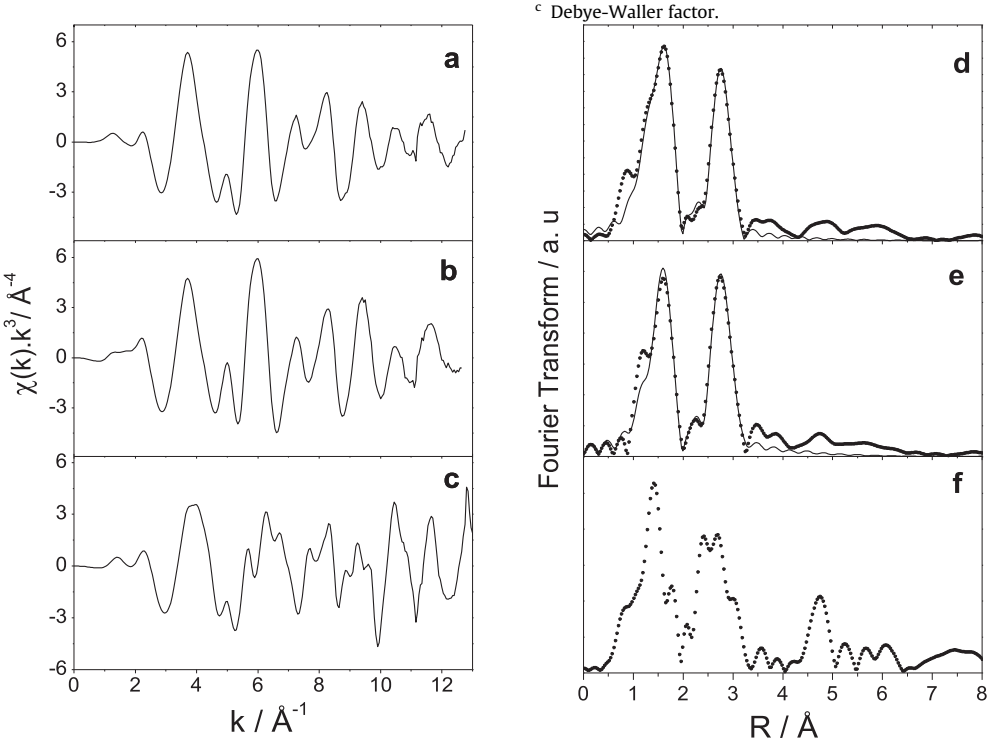

Fig. 6. EXAFS oscillations at the Co K-edge (left) and their corresponding Fourier transforms (without phase correction) (right) of (a), (d) Co/iwi, (b), (e) Co/tie and (c), (f) Co/sc.

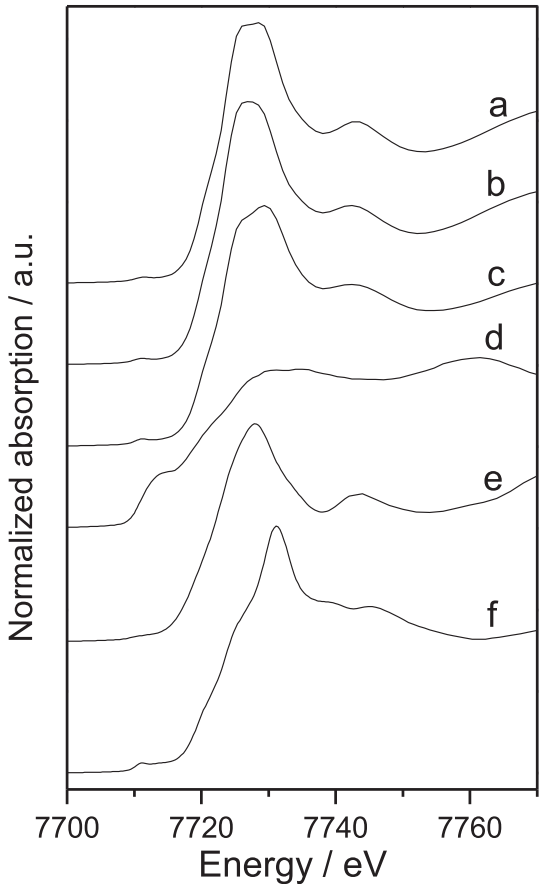

Fig. 7. XANES spectra at the Co K-edge of (a) Co/tie, (b) Co/iwi, (c) Co/sc, (d) Co, (e) CoO and (f) Co_3O_4.

The position of the absorption edge in the XANES spectra can be related to the oxidation state of the absorbing atom [72]. The higher oxidation state of the metal, the more positive the overall charge of the atom, and more energy will be required to excite an electron out of an orbital. Because of this, it is expected that the binding energy of a core electron will increase with the oxidation state and this would be reflected in a shift in the position of the absorption edge to a higher energy. Comparing the position of the absorption edge of the catalysts with the reference compounds, it can be concluded that in every case the oxidation state is Co(II).

Probably, the absence of the corresponding signal of cobalt oxides in the Co/iwi sample is due to the low concentration of these species in the catalyst, as was observed by TPR.

The structure of cobalt atoms in the Co/sc catalyst was determined by component analysis of the XANES spectrum in order to establish if it could be reproduced by a linear combination of known structures. This analysis showed that the XANES spectrum of this catalyst can be reproduced with a combination of the XANES spectra of Co_3O_4 and the Co/iwi catalyst in a ratio 30:70 (Fig. 8). The same procedure can be carried out using the Co/tie catalyst, obtaining the same result. It is important to remember that Co (II) species in interaction with the mesoporous structure were detected in the Co/iwi and Co/tie catalysts. This means that the majority of Co atoms are in high interaction with the MCM41 structure, while a 30% of Co atoms are forming Co_3O_4 nanoparticles. This oxide has the normal spinel structure, in which the Co(II) ions occupy tetrahedral positions and the Co(III) ions occupy octahedral positions in the face-centered cubic oxygen lattice. These results are in agreement with those obtained by TPR, where a peak is reduced at low

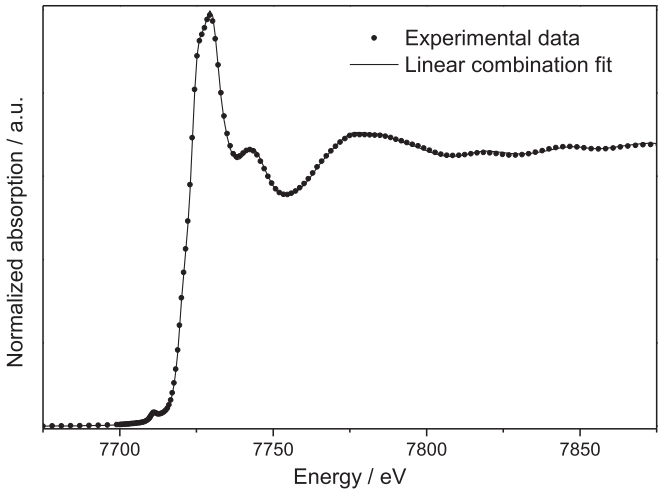

Fig. 8. Linear combination fit of the XANES spectrum of the Co/sc catalyst.

temperature and the Raman signals attributed to Co_3O_4 were observed.

In addition, these results can be supplemented with the surface analysis of the catalysts. X-ray photoelectron spectra were recorded to know the oxidation state and the chemical composition on the surface of Co-MCM41 catalysts. The characteristic core-level spectra of Co 2p, Si 2s, Si 2p are measured. The binding energy (BE) values and the linewidths of Co 2p and Si 2s core-levels and surface atomic ratio of Co/Si are reported in Table 3. All spectra were referenced to C 1s at binding energy of 284.6 eV. The BEs of Si 2p are centered at 103.0 ± 0.1 eV, while for the O 1s region, they are between 532.1 and 532.4 eV in all samples. It is important to note that in the spectral region of the Si 2p there also appears the spectrum of the Co 3s core-level. Because of that, the Si 2s region was also measured, with BEs between 154.0 and 154.2 eV. It was observed that the full-width at a half maximum (fwhm) of Si 2s peaks was wider in samples containing cobalt. Probably, this effect is due to the interaction between the cobalt with the silicon of the structure.

There are few XPS studies of cobalt supported on mesoporous silica structures. However, it is possible to find XPS data about oxides and hydroxides of cobalt which can contribute to identify cobalt species in the present work [72–75].

The XPS spectra of the Co 2p region of the Co/tie, Co/iwi and Co/sc samples are displayed in Fig. 9. The Co 2p spectrum shows different contributions, a spin-orbit splitting into $2p_{1/2}$ and $2p_{3/2}$ components and the shake-up satellites. Therefore, in this study the complete Co 2p spectrum was curve-fitted in order to distinguish the cobalt species present on the material surface.

The spectrum of the Co/tie sample (Fig. 9a) is characterized by the Co $2p_{3/2}$ main peak at binding energy of 781.6 eV and a $2p_{3/2}$-$2p_{1/2}$ splitting of 16.0 eV (see Table 3). As it can be observed, the Co $2p_{3/2}$ main peak has a higher value than those reported in the literature, at *ca.* 780.7 eV for $Co(OH)_2$; 780.0 eV for CoO and 779.9 eV for Co_3O_4 [73,74].I nfantes-Molina et al. [76] studied Co(II) ions interacting with the support as cobalt silicate with the Co $2p_{3/2}$ peak at 781.6 eV.

Fig. 9 (spectrum a) shows a broad intense peak centered at 786.6 eV (Table 3). According to XPS data of cobalt oxides reported in the literature, it is accepted that the chemical shift, the $2p_{3/2}$-$2p_{1/2}$ splitting value ($\Delta E_{1/2\text{-}3/2}$) and the difference between the main peak to the satellite peak ($\Delta E_{mp\text{-}sp}$) contribute to distinguish the oxidation state and coordination of cobalt in the structure. In addition, the satellite peaks appeared at 3.6–6.5 eV above the main peaks $2p_{3/2}$ line. The intensity ratio between main and satellite

Table 3
XPS data of calcined catalysts.

Catalyst	Si 2s/eV	BE Co $2p_{3/2}$/eV		BE Co $2p_{1/2}$/eV		I_{sat}/I_{main} Co $2p_{3/2}$	Co/Si_{surf}
		MainPeak	Satellite	MainPeak	Satellite		
MCM41	154.0 (2.9)[a]	–	–	–	–	–	–
Co/tie	154.0 (3.5)	781.6	786.6	797.6	803.5	0.74	0.20 (0.03)[b]
Co/iwi	154.0 (3.5)	781.5	786.7	797.3	803.2	0.87	0.29 (0.03)
Co/sc	154.0 (3.2)	781.4	786.3	797.4	802.9	0.42	0.04
		779.4	788.9	795.7	805.8		(0.04)

[a] Full width at half maximum (FWHM).
[b] Molar ratio in the bulk.

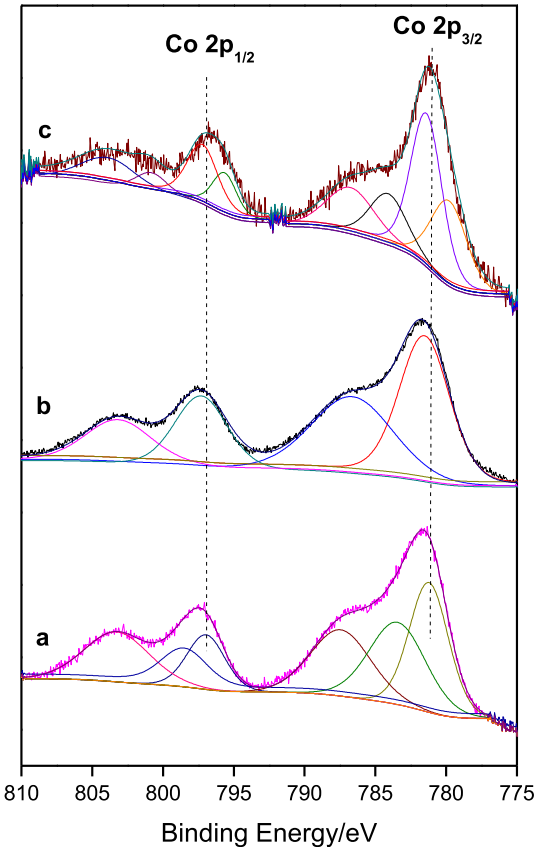

Fig. 9. XPS spectra of (a) Co/tie, (b) Co/iwi and (c) Co/sc catalysts in the Co 2p region.

peak is close to 0.74 and the $\Delta E_{1/2\text{-}3/2}$—16.0 eV.Both parameters are characteristic of Co (II) species [77]. These results are in agreement with the XPS data reported by Mekkiet. al [78], who investigated cobalt sodium silicate glasses. The Co/iwi sample, prepared by the impregnation of cobalt on the MCM41 support, showed a similar spectrum. According to the TPR results, which show that cobalt has a strong interaction with the support, XANES spectra where the Co(II) oxidation state was determined and the XPS measurements, could be consider that cobalt (II) orthosilicate phase is present in the surface of Co/tie and Co/iwi catalysts.

Furthermore, the Co/sc catalyst (Fig. 9c) shows the peaks belonging to Co(II) inside silica framework and, to a lesser extent an additional peaks associated with the formation of the Co_3O_4 spinel, at BEs 779.4–795.7 eV (Co $2p_{3/2\text{-}1/2}$ core-level).

Moreover, the atomic ratios $(Co/Si)_{surf}$ calculated from the XPS data indicate that the cobalt surface enrichment for the Co/tie and Co/iwi catalysts while a homogeneous distribution of cobalt was observed on the Co/sc catalyst. In agreement with this, a lower I_{sat}/I_{main} ratio on the Co/sc catalysts was observed, due to a higher concentration of Co(III) of Co_3O_4.

In summary, it has been possible to identify different cobalt species present in catalysts depending on their synthesis methods. All samples containing a main cobalt species of cobalt (II) coordinated with Si tetrahedral sites form part of mesoporous structure and lesser extent, cobalt orthosilicate on the surface. In addition, Co_3O_4 species dispersed over the MCM41 support were detected for the Co/iwi and Co/sc catalysts.

3.4. Catalytic performance

Fig. 10 shows the CO conversion and selectivity of O_2 towards CO_2 for the total and preferential oxidation of CO over catalysts with cobalt incorporated by different techniques. In the total CO oxidation (COTox) reaction (Fig. 10A-dash line), the 100% CO conversion is reached at 250 °C with the Co/sc sample. However, the Co/tie and Co/iwi catalysts reach a maximum CO conversion of 90 and 78%, respectively. Furthermore, when the preferential CO oxidation (COProx) in a reducing atmosphere was studied (Fig. 10A-solid line), the same trend was observed. This behavior is probably linked to the higher cobalt content in the Co/sc catalyst. The ratio of μmol converted CO/mass of cobalt, (μmol $CO \cdot s^{-1} \cdot g^{-1}$ Co) is estimated, taking into account the CO conversion at 200 °C and considering that all presented cobalt in samples is active. The obtained values for Co/sc, Co/tie and Co/iwi resulted 3.41, 3.46 and 3.85 μmol $CO \cdot s^{-1} \cdot g^{-1}$ Co, respectively. Thus, cobalt oxide spinel and Co(II) species represents active sites for the preferential oxidation reaction of CO in a reducing atmosphere.

Analyzing the oxygen selectivity towards CO_2 (Fig. 10B), it is observed that the curves cross optimum values of 58, 50 and 45% for samples Co/sc, Co/tie and Co/iwi, respectively. Note that when cobalt was added by wet impregnation or the'tie'method, the maximum selectivity value coincides with the maximum temperature of conversion of CO to CO_2 (250 °C). The maximum selectivity for the Co/sc sample was at a slightly lower temperature (200 °C). For all samples, in the region below the maximum value, the selectivity increases with temperature which means that the CO oxidation reaction ($CO + ½\ O_2 \rightarrow CO_2$) was favored. However, above the optimum value, selectivity decreases with temperature indicating that the reaction between H_2 and O_2 is activated to produce water ($H_2 + ½\ O_2 \rightarrow H_2O$). In this sense, this behavior is probably due to the higher contents of cobalt in the sample prepared under supercritical conditions.

Several authors have reported that the Co_3O_4 spinel represents an active phase for the CO oxidation reactions. In this vein, Gómez et al. [79–81] studied the catalytic behavior of Co_3O_4 supported on ZrO_2 and CeO_2 and mixed oxides $MnCoCeO_2$ catalysts in the CoProx reaction. They reported that the Co_3O_4 spinel was the main Co containing compound and it was the active species for the CoProx reaction. Q. Guo et al. [82] reported cobalt supported on mesoporous ceria catalyst (Co_3O_4/meso-CeO_2) for the same reaction. In

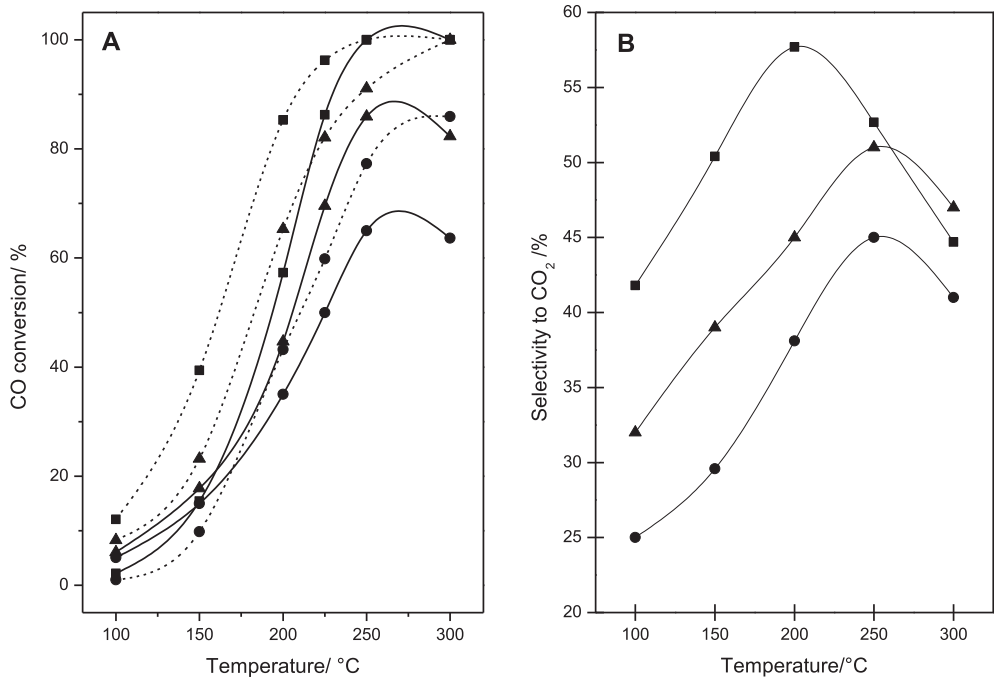

Fig. 10. Catalytic performance of catalysts: ■ Co/sc, ● Co/tie and ▲ Co/iwi. (A) CO conversion, (B) Selectivity of O_2 to CO_2. Reaction conditions: 1% CO, 1% O_2 and/or 40% H_2 in He balance. Catalystweight/total flow: 2.1 mg cm^{-3} min^{-1}. (solid line): COProx, (dash line): COToxreaction.

this case, the authors showed a total CO conversion at 200 °C with 10 and 15 wt % of Co_3O_4.

However, the Co/iwi catalyst exhibits Co(II) ions located in the MCM41 structure, like the Co/tie sample. In this line, Montanari et al. [83] reported the CO adsorption on CoMCM41 and Co-zeolites samples by FTIR. These results show a strong band due to carbonyls on Co(n+) centers. In addition, they reveal evidence of the oxidation of CO to CO_2 due to cobalt species.

In our results, the MCM41 support did not show conversion to CO_2, so that the presence of Co(II) ions represents an adsorption site of CO to improve the oxidation to CO_2.

4. Conclusions

Co-MCM-41 with 4.3 wt % of cobalt synthesized using supercritical CO_2 was the most active and selective catalyst for the preferential oxidation of CO, with total conversion at 250 °C. The Co deposition by the 'scfrd' method contributes with the formation of cobalt oxide nanoparticles (~20 nm) uniformly distributed on the surface and inside of the support. In addition Co(II) incorporated into the MCM41 framework, occupying Si tetrahedral sites was identified. On the other hand, simpler methods for cobalt incorporation cause a significant loss of surface area thus blocking the pores. The incipient wet impregnation (iwi) and ion exchange with the template (tie) methods are performed in aqueous medium, so the hydrolysis and capillary tension exerted by water provoke a damage of the structure. However, the supercritical CO_2 deposition method is less aggressive because it was conducted in dry conditions.

In particular, by 'tie' method the outside of the MCM41 particles represents the area easily exchanged. This effect is linked to a limitation or restriction on the diffusion of cobalt precursor into the structure when begins exchanged ion. In addition, by XPS measurements Co(II) species corresponded to orthosilicate dispersed over the surface of MCM41 were observed for all the samples.

The number of moles converted in relation to the amount of cobalt present in the sample is similar for all samples. Thus, the combination of cobalt oxide Co_3O_4 and cobalt (II) interacting with a siliceous structure, which are highly dispersed on the surface and inside the mesopores, resulted in a highly active and selective catalyst for the preferential oxidation of CO. Incorporating cobalt with supercritical CO_2 leads to a catalyst which produces values of CO conversion similar to those obtained by conventional methods such as incipient wetness impregnation CO. Therefore, the supercritical CO_2 reactive deposition method represents a promising and effective method for incorporating active phases on mesoporous supports.

Acknowledgments

This work was supported by LNLS, Brazil (Project XAFS-18859), UNL (CAI+D 2011), ANPCyT (2013-0354) and CONICET (PIP 112-200801-03079/112-201101-01035). The authors thank ANCPyT for the purchase of the SPECS multitechnique analysis instrument (PME8-2003) and the UV–vis spectrometer (PME 311). Thanks are also given to Fernanda Mori andNuriaNavascuesfor the XPS and TEM measurements, respectively.

Appendix A. Supplementary data

Supplementary data related to this article can be found at http://dx.doi.org/10.1016/j.micromeso.2016.10.006.

References

[1] C.T. Kresge, M.E. Leonowickz, W.J. Roth, J.C. Vartuli, J.S. Beck, Nature 359 (1992) 710–712.
[2] R. Ryoo, M.J. Kim, Chem. Comm. 22 (1997) 2225–2226.
[3] R. Silva-Rodrigo, H. Castillo Jimenez, A. Guevara-Lara, J.A. Melo-Banda, A. Olivas Sarabia, A.I. Reyes de la Torre, F. Morteo Flores, A. Castillo Maresa, Catal. Today 250 (2015) 2–11.
[4] C. Bernal, M. Mesa, M. Jaber, J.L. Guth, L. Sierra, Microp. Mesop. Mater 153 (2012) 217–226.

[5] S. Bhettacharyya, G. Lelong, M.-L. Sabounci, J. Exp. Nanosci. 1 (2006) 375–395.
[6] Y. Wan, D. Zhao, Chem. Rev. 17 (2007) 2821–2860.
[7] I. Sobczak, M. Ziolek, M. Renn, P. Decyk, I. Nowak, M. Daturi, J.-C. Lavalley, Microp. Mesop. Mater 74 (2004) 23–36.
[8] K. Chakarova, et al., Appl. Catal. B Env. 106 (2011) 186–194.
[9] K.-Y. Kwak, M.-S. Kim, D.-W. Lee, Y.-H. Cho, J. Han, T.-S. Kwon, K.-Y. Lee, Fuel 137 (2014) 230–236.
[10] E.G. Vaschetto, G.A. Monti, E.R. Herrero, S.G. Casuscelli, G.A. Eimer, Appl. Catal. A Gen. 453 (2013) 391–402.
[11] L.D. Nguyen, S. Loridant, H. Launay, A. Pigamo, J.L. Dubois, J.M.M. Millet, J. Catal. 237 (2006) 38–48.
[12] D. Wei, W.-T. Chueh, G.L. Haller, Catal. Today 51 (1999) 501–511.
[13] R. Kaur, S.K. Mehta, Coord. Chem. Rev. 262 (2014) 37–54.
[14] K.R. Kloetstra, H. Van Bekkum, Stud. Surf.Sc. Catal. 105 (1997) 431–438.
[15] M. Hartmann, A. Vinu, S.P. Elangovan, V. Murugesan, W. Bohlmann, Chem. Comm. 11 (2002) 1238–1239.
[16] E.R. Leite, N.L.V. Carreño, E. Longo, A. Valentini, L.F.D. Probst, J. Nanosci. Nanotechnol. 2 (2002) 89–94.
[17] N. Bion, F. Epron, M. Moreno, F. Mariño, D. Duprez, Top. Catal. 51 (2008) 76–88.
[18] L.E. Gómez, B.M. Sollier, M.D. Mizrahi, J.M. RamalloLópez, E.E. Miró, A.V. Boix, Int. J. Hydrog. En. 39 (2014) 3719–3729.
[19] L.E. Gómez, I.S. Tiscornia, A.V. Boix, E.E. Miró, Int. J. Hydrog. En. 37 (2012) 14812–14819.
[20] L. Wang, J. Chen, A. Patel, V. Rudolph, Z. Zhu, Appl. Catal. A Gen. 447–448 (2012) 200–209.
[21] S. Huang, K. Hara, A. Fukuoka, Energy Environ. Sci. 2 (2009) 1060–1068.
[22] J.A. Calles, A. Carrero, A.J. Vizcaíno, Microp. Mesop. Mater. 119 (2009) 200–207.
[23] N. Yao, G.X. Xiong, K.L. Yeung, S.S. Yeng, M.Y. He, W.S. Yang, X.M. Liu, X.H. Bao, Langmuir 18 (2002) 4111–4117.
[24] K.S. Hui, C.Y.H. Chao, J. Haz. Mater. B 137 (2006) 1135–1148.
[25] Q. Huo, D.I. Margolese, U. Ciesla, D.G. Demuth, P. Feng, T.E. Gier, P. Sieger, A. Firouzi, B.F. Chmelka, F. Schüth, G.D. Stucky, Chem. Mater 6 (1994) 1176–1191.
[26] J.S. Beck, J.C. Vartuli, W.J. Roth, M.E. Leonowicz, C.T. Kresge, K.D. Schmitt, C.T.-W. Chu, D.H. Olson, E.W. Sheppard, S.B. McCullen, J.B. Higgins, J.L. Schlenker, J. Am. Chem. Soc. 114 (1992) 10834.
[27] J.S. Beck, J.C. Vartuli, G.J. Kennedy, C.T. Kresge, W.J. Roth, S.E. Schramm, Chem. Mater 6 (1994) 1816.
[28] W. Gac, A. Derylo-Marczewska, S. Pasieczna-Patkowska, N. Popivnyak, G. Zukocinski, J. Mol. Catal. A Chem. 268 (2007) 15–23.
[29] M. Yonemitsu, Y. Tanaka, M. Iwamoto, Chem. Mater 9 (1997) 2679–2681.
[30] A.-R. Badiei, L. Bonneviot, Inorg. Chem. 37 (1998) 4142–4145.
[31] Y. Wang, Y. Ohishi, T. Shishido, Q. Zhang, W. Yang, Q. Guo, H. Wan, K. Takehira, J. Catal. 220 (2003) 347–357.
[32] Q. Zhang, Y. Wang, Y. Ohishi, T. Shishido, K. Takehira, J. Catal. 202 (2001) 308–318.
[33] Q. Zhang, Y. Wang, S. Itsuki, T. Shishido, K. Takehira, J. Mol. Catal. A 188 (2002) 189.
[34] M. Yonemitsu, Y. Tanaka, M. Iwamoto, Chem. Mater 9 (1997) 2679–2681.
[35] Y. Sanchez-Vicente, C. Pando, M. Cortijo, A. Cabañas, Microp. Mesop. Mater 193 (2014) 145–153.
[36] A. Cabañas, J.M. Blackburn, J.J. Watkins, Microelect. Eng. 64 (2002) 53–61.
[37] T.A. Crowley, K.J. Ziegler, D.M. Lyons, D. Erts, H. Olin, M.A. Morris, J.D. Holmes, Chem. Mater. 15 (2003) 3518–3522.
[38] E. Reverchon, R. Adami, J. Supercrit. Fluids 37 (2006) 1–22.
[39] J.M. Blackburn, D.P. Long, A. Cabañas, J.J. Watkins, Science 294 (2001) 141–145.
[40] A. Szègedi, Z. Kónya, D. Méhn, E. Solymár, G. Pál-Borbély, Z.E. Horváth, L.P. Biró, I. Kiricsi, Appl. Catal. A Gen. 272 (2004) 257–266.
[41] S.G. Aspromonte, A. Sastre, A.V. Boix, M.J. Cocero, E. Alonso, J. Sup. Fluids 110 (2016) 47–55.
[42] S.G. Aspromonte, A. Sastre, A.V. Boix, M.J. Cocero, E. Alonso, Microp. Mesop. Mater 148 (2012) 53–61.
[43] B. Lippens, B. Linsen, J. de Boer, J. Catal. 3 (1964) 32–37.
[44] L.H. Cohan, J. Am. Chem. Soc. 60 (1938) 433–439.
[45] A. Szegedi, M. Popova, A. Dimitrova, Z. Cherkezova-Zheleva, I. Mitov, Microp. Mesop. Mater 136 (2010) 106–114.
[46] B. Ravel, M. Newville, J. Synchr. Radiat., 12 82005) 537.
[47] S.I. Zabinski, J.J. Rehr, A. Ankudinov, R.C. Albers, M.J. Eller, Phys. Rev. B 52 (1995) 2995.
[48] K.S.W. Sing, D.H. Everett, R.A.W. Haul, L. Moscou, R.A. Pierotti, J. Rouquerol, T. Siemieniewska, Pure Appl. Chem. 57 (1985) 603–619.
[49] M. Park, J.H. Kim, I.-K. Shim, J.-H. Choy, Chem. Eng. J. 253 (2014) 1–7.
[50] C.T. Kresge, M.E. Leonowicz, W.J. Roth, J.S. Beck, Nature 359 (1992) 710–712.
[51] T. Yasmin, K. Müller, Microp. Mesop. Mater 208 (2015) 83–92.
[52] N. Igarashi, K.A. Koyano, Y. Tanaka, S. Nakata, K. Hashimoto, T. Tatsumi, Microp. Mesop. Mater. 59 (2003) 43–52.
[53] L. López Pérez, E.R.H. van Eck, Melian-I. Cabrera, Microp. Mesop. Mater. 220 (2016) 88–98.
[54] Y. Ling, M. Long, P. Hu, Y. Chen, J. Huang, J. Haz. Mater. 264 (2014) 195–202.
[55] M. Shabanian, M. Khoobu, F. Hemati, H.A. Khonakdar, K. Faghihi, U. Wagenknecht, S.E.S. Ebrahimi, A. Shafiee, Particuology 19 (2015) 14–21.
[56] S. Lim, D. Ciuparu, Y. Chen, L. Pfefferle, G.L. Haller, J. Phys. Chem. B 108 (2004) 20095–20101.
[57] A.V. Boix, M.A. Ulla, J.O. Petunchi, J. Catal. 162 (1996) 239–249.
[58] Q. Guo, S. Chen, Y. Liu, Y. Wang, Chem. Eng. J. 165 (2010) 846–850.
[59] Q. Guo, Y. Liu, Appl. Catal. B Env. 82 (2008) 19–26.
[60] N. Li, X. Wang, S. Derroviche, G.L. Haller, L.D. Pfefferle, ACS Nano 4 (2010) 1759–1767.
[61] C. Medina, R. García, P. Reyes, J.L.G. Fierro, N. Escalona, Appl. Catal. A Gen. 373 (2010) 71–75.
[62] B. Boizot, S. Agnello, B. Reynard, R. Boscaino, G. Petite, J. Non-Crystall. Solids 325 (2003) 22–28.
[63] E. Vanea, V. Simon, Appl. Surf. Sci. 280 (2013) 144–150.
[64] J. Llorca, P.R. Piscina, J.A. Dalmon, N. Homs, Chem. Mater. 16 (2004) 3573.
[65] V.G. Hadjiev, M.N. Iliev, I.V. Vergilov, J. Phys, C. Solid State Phys. 21 (1988) L199.
[66] C.-W. Tang, C.-B. Wang, S.-H. Chien, Thermoch. Acta 473 (2008) 68–73.
[67] B.K. Teo, EXAFS: Basic Principles and Data Analysis, Springer-Verlag, Berlin, Germany, 1986.
[68] B. Ravel, M. Newville, J. Synchrotron Radiat. 12 (2005) 537–541.
[69] S.I. Zabinsky, J.J. Rehr, A. Ankudinov, R.C. Albers, M.J. Eller, Phys. Rev. B 52 (1995) 2995–3009.
[70] T. Vrålstad, W.R. Glomm, M. Rønning, H. Dathe, A. Jentys, J.A. Lercher, G. Øye, M. Stöcker, J. Sjöblom, J. Phys. Chem. B 110 (2006) 5386–5390.
[71] T. Vrålstad, G. Øye, M. Rønning, W.R. Glomm, M. Stöcker, J. Sjöblom, Microporous Mesoporous Mater 80 (2005) 291–300.
[72] J.M. Ramallo-López, E.J. Lede, F.G. Requejo, J.A. Rodriguez, J.-Y. Kim, R. Rosas-Salas, J.M. Domínguez, J. Phys. Chem. B 108 (2004) 20005–20010.
[73] M.C. Biesinger, B.P. Payne, A.P. Grosvenor, L.W.M. Lau, A.R. Gerson, R.St.C. Smart, App. Surf. Sci. 257 (2011) 2717–2730.
[74] J. Yang, H. Liu, N. Martens, R.L. Frost, J. Phys. Chem. C 114 (2010) 111–119.
[75] P.N. Shelke, Y.B. Khollaw, K.R. Patil, S.D. Gunjal, S.R. Jadkar, M.G. Takwake, K.C. Mohite, J. Nano-Elect. Phys. 3 (2001) 486–498.
[76] A. Infantes-Molina, J. Mérida-Robles, E. Rodriguez-Castellón, J.L.G. Fierro, A. Jiménez-López, Appl. Catal. B Env. 73 (2007) 180–192.
[77] G.A. Carson, M.H. Nassir, M.A. Langell, J. Vac. Sci. Technol. A 14 (1996) 1637–1642.
[78] A. Mekki, D. Holland, K.H. Ziq, C.F. Mc Conville, J. Non-Crystall. Sol. 220 (1997) 267–279.
[79] L.E. Gómez, A.V. Boix, E.E. Miró, Catal. Today 216 (2013) 246–253.
[80] L.E. Gómez, I.S. Tiscornia, A.V. Boix, E.E. Miró, Appl. Catal. A Gen. 401 (2011) 124–133.
[81] L.E. Gómez, I.S. Tiscornia, A.V. Boix, E.E. Miró, Int. J. Hydrog. En. 38 (2013) 5645–5654.
[82] Q. Guo, M. Wu, Y. Liu, X. Bai, Chin. J. Catal. 28 (2007) 953–957.
[83] T. Montanari, O. Marie, M. Daturi, G. Busca, Catal. Today 110 (2005) 339–344.